Check for updates

Performance of Graphene Derivatives Produced by Chemical and Physical Methods as Reinforcements in Glass Fiber Composite Laminates

Lourdes Ramos-Galicia[1] · Christian Daniel Reyes-Vazquez[1] ·
Ana Laura Martínez-Hernández[1] · Julio Alejandro Rodríguez-González[2] ·
Carlos Rubio-González[2] · Armando Almendarez-Camarillo[3] · Carlos Velasco-Santos[1]

Abstract

In this work, graphene derivatives obtained by a common chemical method and a novel physical route are evaluated as reinforcement nanomaterials on prepregs based on glass fiber and epoxy resin. Besides, two types of graphite were employed to obtain graphene derivatives, through the chemical route, and to evaluate the influence of their structure quality on the performance of the composite laminates prepared. All graphene derivatives were characterized by different techniques and specific structural features were found depending on processing method; less structural damage in the graphene derivatives obtained by steam explosion and ultrasonication (physical route) was observed. Graphene derivatives were incorporated on the surface of prepregs, which were laminated to evaluate their performance through short beam tests and dynamic-mechanical analysis. Carbon materials obtained by the physical route produced remarkable thermomechanical performance, and also, better interfacial properties in the composite laminates compared to that observed with graphene oxide and reduced graphene oxide obtained from the two kinds of graphite precursor.

✉ Carlos Velasco-Santos
cylaura@gmail.com

1   División de Estudios de Posgrado e Investigación, Tecnológico Nacional de México/
    Campus Querétaro Avenida Tecnológico S/N Esq. Gral Col. Centro Histórico,
    Qro C.P. 76000 Mariano Escobedo Querétaro, Mexico

2   Centro de Ingeniería y Desarrollo Industrial, Av. Pie de la Cuesta #702, Col. Desarrollo San
    Pablo, C.P. 76125 Querétaro, Qro, Mexico

3   Departamento de Ingeniería Química, Tecnológico Nacional de México/Campus Celaya, Av.
    Tecnológico Y Antonia García Cubas, C.P. 38010. Celaya, Fovissste, Guanajuato, México

1 Introduction

Graphene has been one of the most investigated materials around the world since its discovery in 2004. From this moment, a enormous quantity of studies for its production were proposed, resulting a variety of graphene derivatives [1]. Chemical methods were mentioned as ones with high possibilities for mass production [2, 3]. This route starts from graphite which is oxidized and exfoliated to obtain graphene oxide (GEO). Graphene oxide contains some oxygen groups in the plane and others at the edges [4, 5], which change the surface character to hydrophilic [6–8]. Even when researchers have demonstrated that these functional groups are useful for attaching additional molecules or bonding to different polymer matrices [9–11], some properties are affected due to the formation of sp^3-carbons disrupting the conjugated π-electron system [12]. For the restoration of the graphitic lattice, a reduction process can be realized through a variety of chemical agents [4], resulting reduced graphene oxide (RGO). This nanomaterial recovers only partially its sp^2 hybridized π-network [13], and becomes hydrophobic again. The structure quality of graphene oxide and reduced graphene oxide decreases compared to the precursor, however, they have been evaluated for diverse areas and were found suitable for many applications, such as reinforced materials [14]. On the other hand, chemical vapour deposition represents a methodology to obtain monolayers of graphene, but some studies mention the complexity of the process and high cost [15]. Mechanical milling of graphite has been probed to produce few-layer graphene sheets modifying the milling time, liquid media, speed of rotation, size of milling balls, among others [11, 16, 17]. Nevertheless, the graphitic lattice is damaged during the milling and the process consumes a lot of energy and takes long time, therefore it remains at laboratory level [11]. Liquid phase exfoliation of graphite is mentioned as a potentially scalable method to produce from single, few-layer graphene, to graphene nanoplatelets (GNPs), but the main limitation is the corrosive, expensive, and toxic solvents needed for overcoming the van der Waals forces in graphite layers [18, 19]. Water has been used as a solvent in presence of surfactants or polymers to modify its surface tension, however, these additional molecules could appear as impurities in the final materials [20]. Recently, steam explosion followed by an ultrasonication stage has been proposed by our research group to obtain graphene nanoplatelets (more results of GNP at different conditions would be published elsewhere, in a journal related to physical and chemical structure of materials). Steam explosion usually is employed for treating biomass at pressurized steam and high temperature during a period of time for a sudden decompression stage [21]. This process has been probed using graphite instead biomass, later the steam-exploded graphite (EG) is ultrasonicated to diminish the number of graphene layers and obtain exfoliated and steam-exploded graphite (EEG) or also named graphene nanoplatelets. It was observed that both stages did not damage significantly the graphitic lattice, under these conditions, and no impurities were added because only water was used during the whole methodology. Therefore, these materials are interesting for evaluation of their performance, especially as reinforcement in composites, due to this being one of the most important industrial applications.

Diverse graphene derivatives have been used as reinforcement in different polymer matrices [22–26], especially in fiber reinforced plastics (FRPs) [27–29]. FRPs based on epoxy resin are continuously studied due to the wide application in high performance components [30]. The main problem of these materials is their delamination, risking the mechanical resistance and their structural integrity [31–33]. To overcome this issue, in the last years, graphene derivatives have been incorporated in these systems to increase the interfacial adhesion. Distinct

graphene materials have been introduced into the matrix and this mix impregnated onto the fibers [28, 34]. Other form for incorporating graphene derivatives is as a coating onto the fibers for a subsequent infusion with the resin [35]. Moreover, carbon nanolayers have been attached to fibers [36]; or in other works, between every layer of the composite laminate [37]. Some of these graphene derivatives are displayed in Table 1. They were employed in recent works and the resultant effect of reinforcement, to a large degree, depended on the structural features of carbon nanolayers and the reinforced region of the FRPs. In this Table, important differences are observed between the graphene derivatives, and these characteristics are usually obtained from the method of production, which diversify the results when the composite laminates are characterized. The presence of graphene derivatives in FRPs can produce increments in the interfacial adhesion, higher impact resistance, major flexural strength, improvement in inter-laminar fracture toughness [29, 32, 38, 39], among others. Therefore, new methods to produce graphene derivatives with excellent properties and feasible scale-up are necessary, because of real industrial application in FRPs, requires the sufficient supply of this nanomaterial [40, 41].

In this work, the evaluation of graphene derivatives obtained by chemical and physical methods is presented; and the last route presents the advantage of being environmentally friendly because only water is used in the whole process. It is important to highlight that methodologies used to obtain graphene derivatives, like graphene oxide or reduced graphene oxide, are more complex in their process and employ reagents which are not environmentally friendly and cause damage to the graphitic structure. Regarding graphene nanoplatelets, several proposed routes also cause damage to the material structure and some impurities are found in the product; therefore, new options are needed to be explored. Moreover, compared to other methodologies, the physical route employed here, is feasible for scale-up, green, easy in their process, able to supply large quantities of product, uses only water, and through the process it is possible to modify the thickness of the material, which could influence the properties of the composite laminates. The effect of reinforcement of the starting graphite is evaluated to compare this performance with the materials obtained after each process of the physical route. On the other hand, it has been reported that GEO and RGO produce improvements in FRPs (see Table 1); therefore, their performance is contrasted with that obtained by graphene derivatives from the new physical method, under the same process conditions. Besides, for the production of graphene oxide and reduced graphene oxide, two graphite precursors were employed in order to study the quality effect on the features of the final nanomaterials as reinforcements. One type was highly oriented pyrolitic graphite (HG) used for microscopy, and its cost is around 600 US$ per kg; and the other was natural graphite (NG) of lower orientation respect to the first one, whose cost is 10 US$ per kg, approximately. Natural graphite was selected for physical treatments and obtaining new graphene derivatives due to a considerable quantity was required during the process and its low cost let to real-ize the production. After characterizing the whole nanomaterials, they were evaluated as reinforcements in composite laminates through interlaminar shear strength and dynamic mechanical tests.

2 Materials and Methods

2.1 Materials

Graphene oxide and reduced graphene oxide were prepared from two graphite precursors: a) graphite roads No. 70230 from Electron Microscope Sciences (USA) with 2 ppm or

Table 1 Graphene derivatives incorporated as reinforcement in FRPs

Type of graphene derivative	Type of FRPs	Load of graphene derivative	Reinforced region of the FRPs	Evaluation of reinforced FRPs and improvements respect to the unreinforced composite laminates	Reference
GEO, thickness around 1–2 nm	Carbon fiber/epoxy	--	GEO reinforced epoxy inter-leaf into the interface of FRPs	Mode-I fracture toughness and resistance: 170.8% and 108%, respectively	42
Commercial graphene	Carbon fiber/poly(ether ether ketone)	0.3–1.0 wt.%	Poly(ether ether ketone matrix	Thermal conductivity: 53.7% Tensile strength similar to the reference specimen Flexural strength: ~5%	43
GEO	Glass fiber/epoxy	0.05, 0.1, 0.2 wt.%	Epoxy matrix	Flexural strength: 30% Flexural modulus: 21%	34
GNPs, 5–15 nm of thickness	Carbon fiber/epoxy	0.25, 0.50, 0.75 wt.%	Epoxy matrix	Interlaminar shear strength: 17% Mode I fracture toughness: until 93.4%	44
GNPs, 6–8 nm of thickness	Glass fiber/epoxy and carbon fiber/epoxy	--	Epoxy matrix	Impact energy absorption capacity of glass/epoxy laminates: 3.5% Impact energy absorption capacity of carbon/epoxy laminates: 4.5%	45
Two different dimensions of GNPs, diameter < 1 μm and ~5 μm, both thickness of 5–7 nm	Glass fiber/epoxy	3.0, 5.0 wt.%	Epoxy matrix	Flexural strength: until 16.2% Flexural modulus: until 26.3% Storage modulus at 30 °C: until 28.2%	38
RGO	Carbon fiber/epoxy	0.5, 1.0 wt.%	Graphene/epoxy as interleaves	Mode I interlaminar fracture energy: 140% Matrix fracture energy: ~150% Reduction of the thermal expansion coefficient: ~30%	46

Table 1 (continued)

Type of graphene derivative	Type of FRPs	Load of graphene derivative	Reinforced region of the FRPs	Evaluation of reinforced FRPs and improvements respect to the unreinforced composite laminates	Reference
GEO, 2–4 nm of thickness	Carbon fiber/epoxy	0.05, 0.10, 0.20, 0.40 wt.%	Epoxy matrix	Interlaminar shear strength: 8.05% / Glass transition temperature: ~2.3%	47
GNPs, 5–17 nm of thickness	Carbon fiber/epoxy	5.0 wt.%	Epoxy matrix	Flexural modulus: 15% / Interlaminar shear strength: 18% / Out-of-plane electrical and thermal conductivity: two orders of magnitude and 50%, respectively	48
GEO	Carbon fiber/epoxy	--	Surface of the carbon fibers	Interlaminar shear strength: 58.6% / Moisture absorption decreased by 63.6%	49
GNP (15 nm of thickness)-phenolic resin mix	Carbon fiber/epoxy	1.25 wt.%	Surface of the carbon fibers	Interlaminar shear strength: 37.04% / Thermal conductivity: 16.67%	50
GEO	Carbon fiber/epoxy	0.25 wt.%	Prepreg surface	Mode I interlaminar fracture toughness: 8% / Mode II interlaminar fracture toughness: 8% / Interlaminar shear strength: ~3%	37
Commercial GEO, RGO, GNPs (1.5 nm of thickness)	Glass fiber/epoxy	0.22, 0.44, 0.88, 1.32, 1.85, 2.2 vol.%	Epoxy matrix and the surface of fibers	Thermal conductivity until 12.6% with GNPs	51

Table 1 (continued)

Type of graphene derivative	Type of FRPs	Load of graphene derivative	Reinforced region of the FRPs	Evaluation of reinforced FRPs and improvements respect to the unreinforced composite laminates	Reference
GEO, dodecylamin-GEO, 1-(3-aminopropyl) imidazole-GEO	Glass fiber/epoxy	0.5 wt.%	Epoxy matrix	Mode I interlaminar fracture toughness: until 28.3% Storage modulus: until 59%	52
GEO	Carbon fiber/epoxy	0.14, 0.27, 0.54, 1.08, 1.63, 2.71 vol.%	Epoxy matrix	Interlaminar shear strength: until 58.4% Electrical and thermal conductivity in the through-thickness direction: 231.5 and 7.8%, respectively	53
GNPs, 5 nm of thickness	Carbon fiber/epoxy	0.1, 0.3, 0.5 wt %	The fiber surface	Flexural strength: until 27.2% Interlaminar shear strength: until 24.5% Thermal conductivity until 55.6%	32

less of impurities, and b) natural graphite powder from Reactivos Química Meyer (MEX); this last one was also employed for the steam explosion process. Ethyl alcohol absolute anhydrous (CH_3CH_2OH, 99.95%) for spraying nanomaterials was acquired from J.T. Baker (USA). Unidirectional glass fiber/epoxy prepreg (DA 409 U/S2-Glass) (resin content: 38% by weight) was supplied by Adhesive Prepregs for Composite Manufacturers (USA). Diglycidyl ether of bisphenol A (DGEBA, D-3415, molecular weight of 60.1 g/mol) was acquired from Sigma-Aldrich, for dispersion tests.

2.2 Preparation of Nanomaterials and Composite Laminates

Highly oriented pyrolitic graphite (HG) and natural graphite (NG), were used as precursors for graphene oxide, obtained by modified Hummers method and sonication, considering a previous research [54]. Graphene oxide based on highly oriented pyrolitic graphite (H-GEO) and natural graphite (N-GEO), respectively, were reduced using ascorbic acid according to previous methodologies [55] to produce reduced graphene oxide (H-RGO and N-RGO depending on the graphite precursor).

    With regard to the physical method, only NG was employed due to N-GEO showing comparable performance to H-GEO (see results and discussion section); in addition, it is considerably cheaper than HG. Moreover, considering that the method is closer to scale up, the material quantity is an important factor. 100 g of NG and 4000 mL of distilled water into the steam explosion equipment was introduced. The conditions for steam explosion were 170 °C and 130 PSI, and the process was carried out during 30 min. Then, the camera was depressurized and the steam-exploded solid was dried at 70 °C after
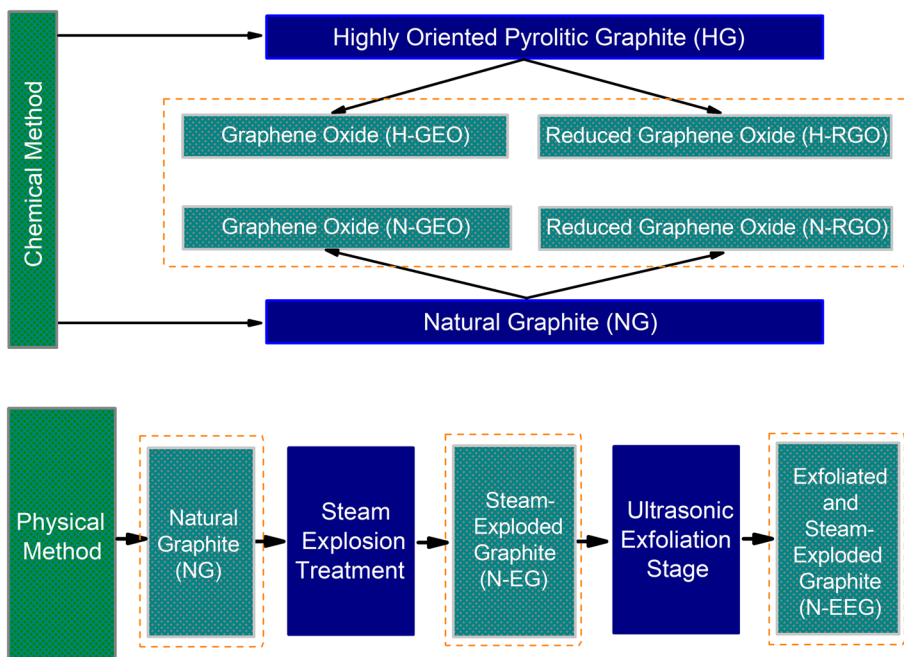

Fig. 1 Graphene derivatives prepared in this work as reinforcement of GFRPs

a decantation stage to eliminate the excess of water. The dried powder corresponds to steam-exploded graphite, N-EG. Then, 200 mg of N-EG were mixed with 20 mL of distilled water and sonicated using a tip (AS Serial Ultrasonic Cleaner, AS7240B) during 80 min. The dispersion was dried at 70 °C to obtain exfoliated and steam-exploded graphite, N-EEG. In this work, 30 min of steam explosion were employed to keep low costs and major posibilities to scale up and use of this route. The set of nanomaterials prepared in this work for reinforcing composite laminates are showed in Fig. 1.

Unidirectional glass fiber/epoxy prepreg was sprayed (using an airbrush) on one side with a dispersion of ethanol and a kind of graphene derivative (H-GEO, H-RGO, N-GEO, N-RGO, NG, N-EG, or N-EEG) to form a composite of 16 layers. Carbon materials were distributed at the 15 interfaces of each composite laminate. Low concentrations of graphene derivatives were employed, 0.05, 0.15, and 0.3 wt.% to avoid excessive agglomeration on the prepregs'surface. Composite laminates with and without reinforcements were developmented using the vacuum bag technology and cured according a previous work [37].

2.3 Characterizations

All powder samples of graphene oxide and reduced graphene oxide were characterized by infrared spectroscopy (IR) in a FT-IR Bruker Vector 33 spectrometer (1 cm^{-1}) in attenuated total reflection mode. Raman spectra were obtained through a Senterra Bruker Raman spectrometer with a resolution of 4 cm^{-1} and a laser of 785 nm. Micrographs were obtained using a JEOL TEM-1010 microscope functioning at 80 kV. Graphene derivatives obtained by the physical route were analyzed by IR spectroscopy, and transmission electron microscopy (TEM) with the specification above mentioned. Moreover, X-Ray diffraction (DRX) was employed in order to calculate the number of layers of the nanomaterials, through a X-Ray diffractometer Rigaku, from 0 to 60 in 2θ angle. Moreover, dispersion in solvents of all graphene derivatives prepared in this work was evaluated. The objective of these tests was to analize their dispersion facility, stability and compatibility of these materials in different solvents, specially epoxy resin. Dispersion is an important factor for the performance of the reinforcements; therefore, it was necessary to evaluate the tendency of each material, which depends on their surface properties, and these features are influenced by the type of used precursor and the obtaining method. For these tests, 4 mg of each carbon nanomaterial and 20 ml of solvent (distilled water, DGEBA, and hexane) were mixed and sonicated for 10 min. The evolution of dispersion was followed at different time.

Composite laminates with and without reinforcements were evaluated by short beam shear test under the ASTM D2344 methodology. Five specimens of (40*12*3.8) mm were tested with a Instron 8872 testing machine at 1 mm/min. Dynamic mechanical analysis (DMA) was carried out using a DMA-8000 Dynamic Mechanical Analizer (PerkinElmer) in dual cantiever mode at a frequency of 1 Hz, from 40 to 200 °C at 5 °C min^{-1}. Specimens of (45*10*3.8) mm were evaluated to obtain the storage modulus and tan delta graphics. The delaminated regions of the specimens were covered with gold and analyzed through a JEOL JSM-6060LV microscope operating at 20 kV.

2.4 Results and Discussion

2.4.1 Graphene Derivatives Produced by the Chemical Method

The infrared spectra of graphene derivates are presented in Fig. 2a, b. Notable differences are observed for all materials, from graphite precursors until reduced graphene oxide. First, natural graphite (NG) contains oxygen, which is evidenced by the band at 990 cm^{-1} generated by the stretching vibration of C-O. HG does not exhibit this band, only around 1622 cm^{-1} caused by the stretching vibration of C=C; therefore, this highly oriented graphite does not contain oxygen. The graphene oxide obtained from these graphite precursors presents peaks corresponding to specific groups. For H-GEO, it is clear the formation of hydroxyl groups (-OH) which generates the wide band from 3100 to 3500 cm^{-1}, and the peak at 1720 cm^{-1} is consecuence of the stretching vibration of C=O groups from de carboxyl groups [56]. The stretching vibration of C=C is observed at 1600 cm^{-1}, whereas the bands at 1228 and 1058 cm^{-1} are caused by the stretching vibration of (C-O) associated to phenol and epoxy groups [54], respectively. On the other hand, the spectrum of graphene oxide obtained from natural graphite exhibits, mainly, bands at 1719, 1600, 1400, and 990 cm^{-1} attributed to the stretching vibration of C=O from carboxylic groups, C=C, C=O due to carboxylate groups and C-O groups [7, 54]. The presence of oxygen in NG
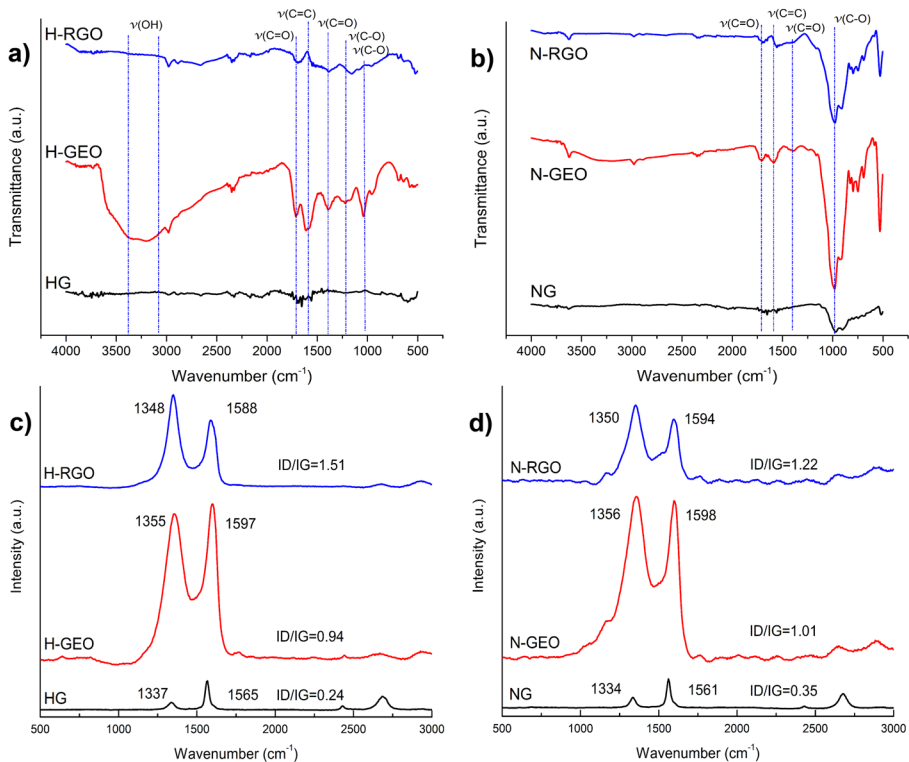

Fig. 2 Infrared (**a,b**) and Raman (**c,d**) spectra of graphene derivatives obtained by the chemical method from two types of graphite, HG, and NG

and its lower orientation degree respect to HG, could stimulate the formation of certain oxygen groups observed in the spectrum, such as carboxylic instead of hydroxyl groups. Then, the structural characteristics of the graphite precursor have influence on the concentration and type of oxygen groups formed on graphene oxide.

With regard to reduced graphene oxide, it has been extensively reported that the restoration of the graphenic domain is not complete employing chemical methods [57]. For H-RGO most of the peaks disappear due to the reduction process and some weak bands are observed owing to the oxygen remainder, such as carboxylic, carboxylate, and phenol groups (1700 cm^{-1}, 1400 cm^{-1}, and 1190 cm^{-1}). Regarding N-RGO, the peaks presented in the spectrum are smaller compared to those observed for N-GEO, their intensity implies a reduction on the quantity of oxygen residual. Therefore, the use of NG produces graphene oxide and reduced graphene oxide with certain groups and a major content of oxygen. It is probable that the low orientation between the sheets allows more contact between the graphitic materials and the reactives which promotes the formation of the functional groups observed at higher concentration compared with the graphene derivatives obtained from HG.

The structural analysis was realized through Raman spectroscopy and the spectra are showed in Fig. 2c, d. Typical bands on carbon materials are observed such as G band at ~ 1580 cm^{-1} arised by in-plane vibration of sp^2 atoms [58], and D band at ~ 1350 cm^{-1} is related to disorder and local defects in the graphenic domain. Besides, at ~ 2700 cm^{-1} the 2D peak appears, which is due to second order zone boundary phonos [6]. It is observed for both graphene oxide samples that D band increases significantly and the G peak becomes broader, respect to graphite spectrum, due to the presence of oxygen generated in the oxidation process. Additionally, both H-GEO and N-GEO, exhibit shifted G bands to higher wavenumbers (from 1565 to 1597 cm^{-1}, and from 1561 to 1598 cm^{-1}, respectively) and the 2D peak decreases, this last by the delamination of the materials. The changes in the bands are caused by the partial amorphization of graphitic lattice, which is calculated through the ID/IG ratio. For both graphene oxide samples, this value increases considerably compared to that calculated on each graphite precursor, from 0.24 to 0.94 for H-GEO, and 0.35 to 1.01 for N-GEO. NG presents higher structural disorder than HG, due to its nature; therefore, N-GEO is affected by the initial structural condition and the ID/IG ratio evidences this features. Otherwise, for both reduced graphene oxide samples, D and G peaks shift to lower frequencies toward those observed in graphite precursors indicating a partial restoration of the sp^2 domains, in spite of by chemical methods the recovery of the graphitic lattice is not complete. The increment on ID/IG values for both reduced graphene oxide is explained by the numerous new in-plane sp^2 domains and smaller average crystallite size [59], implying that H-RGO presents more domains created by the reduction process.

The morphological characteristics of the oxidized and reduced nanolayers are showed in Fig. 3a-d. All graphene derivatives are highly transparent, implying they are conformed by few layers as result of their exfoliation after the oxidation process. Even though no obvious differences are distinguished between the samples, sheets of different sizes were found and all of them exhibited a wrinkled surface which avoid the restacking of the layers [23]. These micrographies confirm the decrease of the number of layers implied in Raman results through the 2D band reduction for graphene oxide and reduced graphene oxide from two precursors.

Figure 4 shows the dispersion tests, of graphene oxide and reduced graphene oxide produced from HG y NG, respectively. H-GEO and N-GEO are well dispersed in distilled water the first minutes (Fig. 4a, b). It is observed that N-GEO exhibits a darker color than H-GEO mixture, which is an indicative of a better dispersion. This is due to the higher
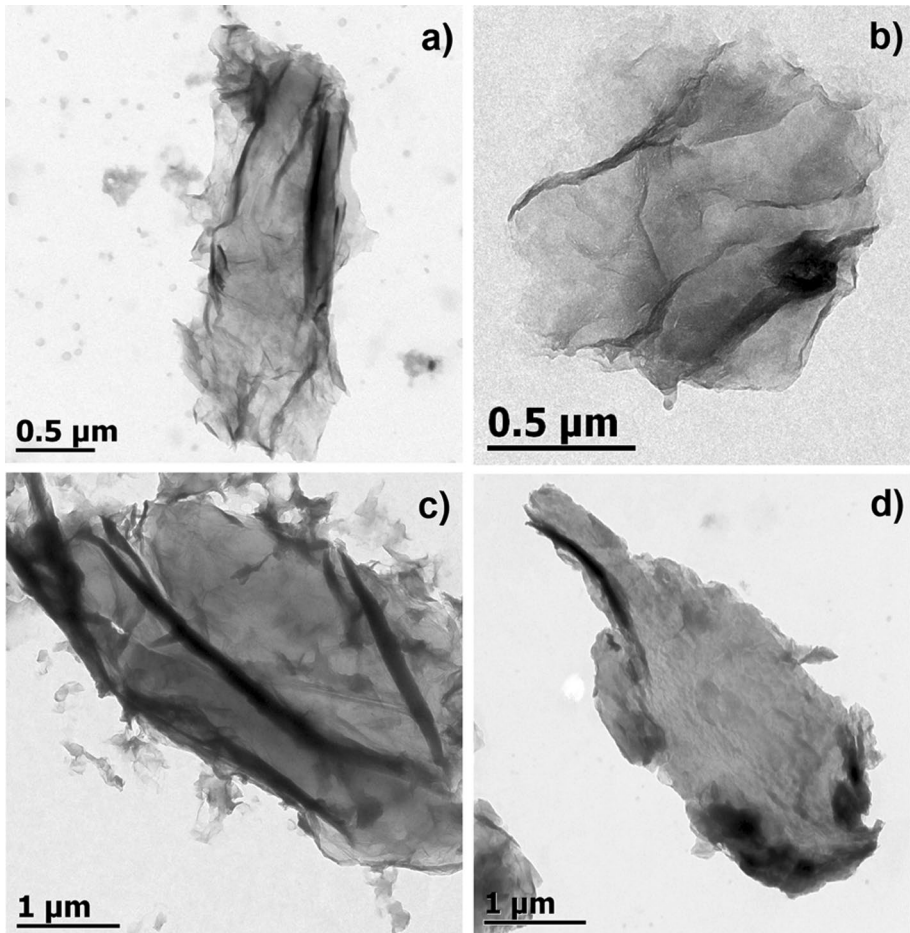
Fig. 3 TEM images of the graphene derivatives obtained by the chemical method: **a**) H-GEO, **b**) N-GEO, **c**) H-RGO, and **d**) N-RGO

oxygen content in N-GEO; the structural quality and the oxygen contained in NG (discussed in IR and Raman section) favored a higher oxidation degree. However, after 48 h both powder formed sediments. H-GEO and N-GEO dispersed in DGEBA (Fig. 4c, d) remained similar after 48 h, but a low quantity of the nanomaterials were observed at the bottom of the containers. The mixtures with hexane (Fig. 4e, f) formed sediments instantly due to graphene oxide being hydrophilic. On the other hand, H-RGO and N-RGO were dispersed in distilled water (Fig. 4u, v) and the mixtures are slightly clearer than those observed for the graphene oxide samples. Reduce graphene oxide recovers its hydrophobicity as a consequence of the restoration of its graphitic lattice; therefore, its dispersion in water decreases. When H-RGO and N-RGO are incorporated in DGEBA (Fig. 4w, x), mixtures are darker than those obtained in water; reduced graphene oxide can be dispersed in the epoxy resin, which is also hydrophobic. Nevertheless, N-RGO is dispersed in higher degree than H-RGO, as it is exhibited in the mixture through its darker color. These powders with hexane were totally separated after 2 h (Fig. 4y, z).
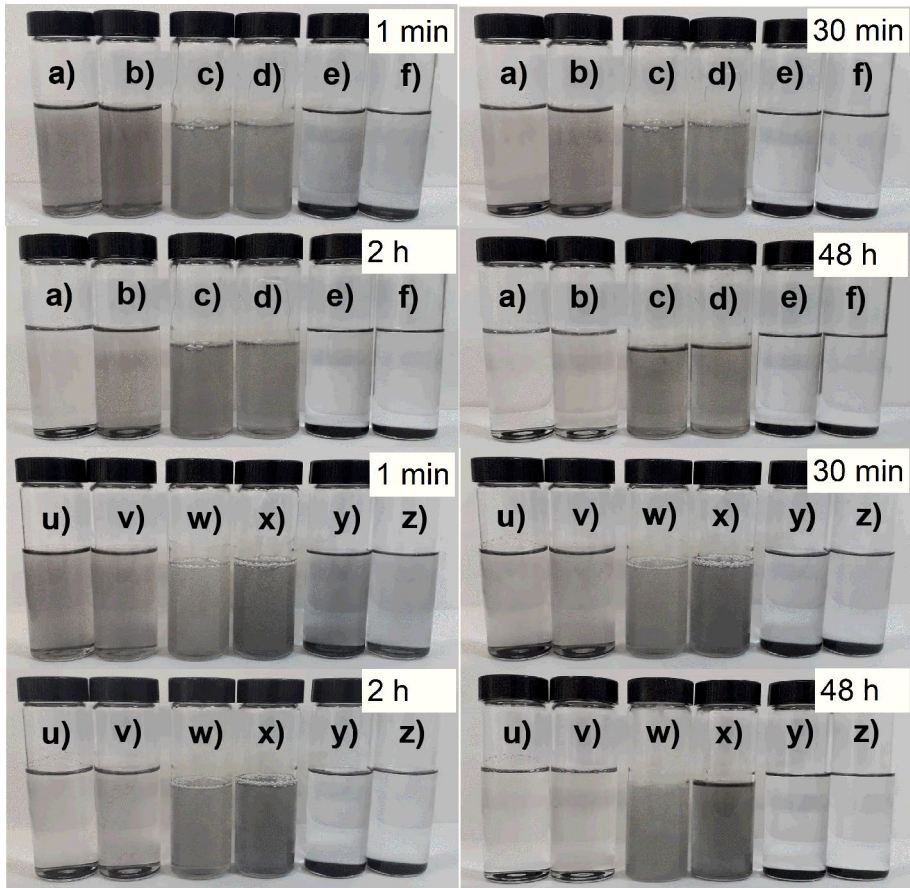
Fig. 4 Dispersion tests using distilled water with **a**) H-GEO, **b**) N-GEO, **u**) H-RGO, **v**) N-RGO; DGEBA with **c**) H-GEO, **d**) N-GEO, **w**) H-RGO, **x**) N-RGO; and hexane with **e**) H-GEO, **f**) N-GEO, **y**) H-RGO, **z**) N-RGO

2.5 Graphene Derivatives Produced by the Physical Route

The infrared spectra of steam-exploded graphite, and exfoliated and steam-exploded graphite are observed in Fig. 5a. It was noted the presence of oxygen in NG discussed in the previous section. The procedure does not promote formation of additional oxygen groups. The infrared spectra of N-EG and N-EEG do not exhibit new bands additional to the graphite precursor, therefore, steam explosion and the exfoliation at these conditions do not generate functionalization of the graphitic lattice. This is remarkable because the structural characteristics of the material remain almost similar to the precursor.

On the other hand, interplanar d-spacing, as well as the number of layers conforming N-EG and N-EGG were determined through XRD patterns (Fig. 5b). The intense peak observed around 26.4 is the (002) reflection related to the ordered graphite [60]. Some changes were produced in this peak respect to that obtained for NG. From the diffractograms it was possible to calculate the distance between graphene layers employing the Bragg's Law [60]. According to this result interplanar d-spacing remains similar, around 0.337 nm,
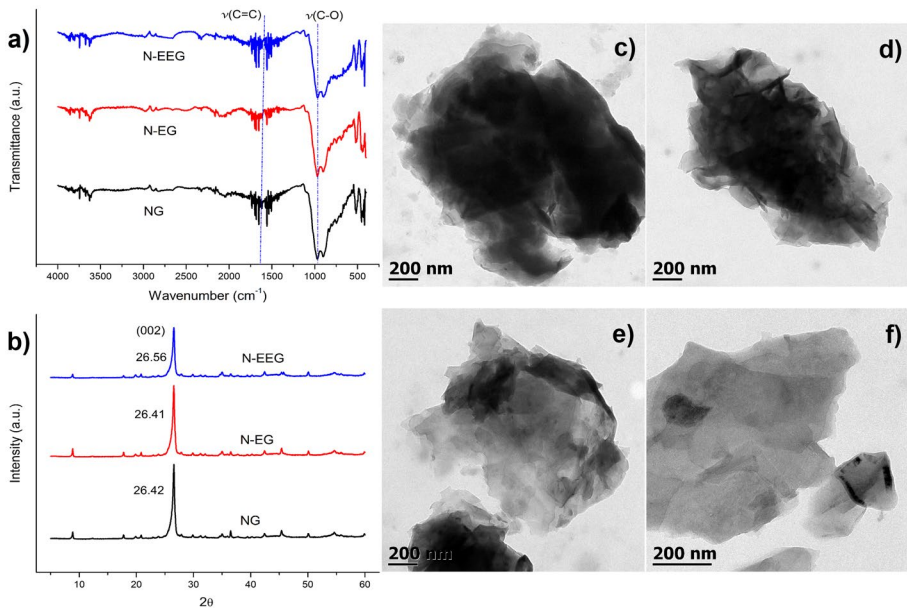
Fig. 5 Infrared spectra **a**) and XRD diffraction pattterns **b**) of graphene derivatives obtained by the physical route produced from NG. TEM images of NG **c**), N-EG **d**), and N-EEG (**e**, **f**)

for N-EG, and N-EEG. This is expected due to new oxygen groups not being generated by these processes, which is corroborated through infrared spectra previously discussed. Also, mean size of the thickness for the treated materials were calculated using Scherrer's equation and taking the interlayer distance, the number of layer was obtained for N-EG, and N-EEG. It was found that steam-exploded graphite is shaped by 76 layers, which corresponds to~26 nm of thickness. After sonication, N-EEG is conformed by 58 sheets, around~19 nm of thickness. Although both carbon materials are in nanoscale range, N-EEG posses lower thickness and this feature could play an important role in the final properties. Hence, this methodology involving two stages, steam explosion and ultrasonication, is a feasible proposal because the structural quality of the materials is similar to the precursor, no additional functional groups are generated, and thickness as low as 19 nm is reached; besides, it is environmental friendly because only water is used during the entire process.

Figure 5c-f displays micrographs of NG, N-EG, and N-EEG. For NG, note its high thickness through the intense darkness caused by all the stacked layers in this material. After steam explosion, the material is slightly more transparent especially at borders, which could be due to a small displacement between sheets; even some morphological details of graphene layers are observed, such as wrinkled surface. In regard to N-EEG, some nanoplatelets with high transparency are found caused by the ultrasonication stage. Some darkness regions are observed; although with the exfoliation lower thickness was obtained respect to N-EG, the main stacked sheets results in 19 nm. However, TEM images showed noticable changes produced by the two stages applied to NG.

Figure 6 exhibits the dispersion tests of graphene derivatives obtained by the physical method. NG, N-EG, and N-EEG in distilled water are well dispersed during the first minutes, especially N-EG and N-EEG (Fig. 6a-c). These three materials produced darker mixtures compared to those obtained with the previously discussed graphene oxide or reduced graphene

oxide. The black dispersions with N-EG and N-EEG corroborate the decrement of the lay-
ers in NG after steam explosion and exfoliation stages. Sediments of NG were observed
after 48 h; N-EG and N-EEG also form sediments, however, a certain quantity of these
materials remain dispersed. Even when the oxygen content in these materials is low, the
powders are well dispersed in water. Through this methodology, the resultant materials are
formed by ~ 26 and ~ 19 nm of average thickness, but probably few layers are also produced
and they may contribute to the good dispersion observed. Mixtures with DGEBA were
stable during the 48 h analyzed (Fig. 6d-f). In fact, the darkest dispersions were obtained
with the incorporation of NG, N-EG, and N-EEG into the epoxy resin, which makes evi-
dent the good compatibility between the phases. When hexane is used as a solvent, the
materials remain well dispersed for some minutes (Fig. 6g-i). Their hydrophobic character
makes dispersion possible in this medium, although it prevailed during a period of time, 2 h
later sediments were observed.

2.6 Composite Laminates Characterization

2.6.1 Short Beam Shear Tests

The prepared nanomaterials by the chemical route present certain characteristics, graphene
oxide samples are hydrophilic and reduced graphene oxide samples are hydrophobic;
besides they were obtained from precursors of different structural quality. These features
mark determined tendency on the interlaminar shear strength (ILSS) results (Fig. 7a-
b). ILSS values were calculated from the load–displacement curves (Fig. 7c-d) accord-
ing to previous reports [47]. The load–displacement curves exhibit a linear region around
0.1–0.5 mm of displacement; thereafter a non-linear region is observed and the maximum
load is distinguished. Then, the load decreased due to the interlaminar damage evolution
[61]. The maximum load detected is associated with the failure load and employed to obtain
the interlaminar shear strength values of the specimens. In general, both reduced graphene
oxide types exhibit higher performance as reinforcement than graphene oxide samples
(Fig. 7a). Even when the graphitic domain restoration is partial, it seems that H-RGO and
N-RGO are more compatible with the epoxy polymer of prepregs. It has been mentioned
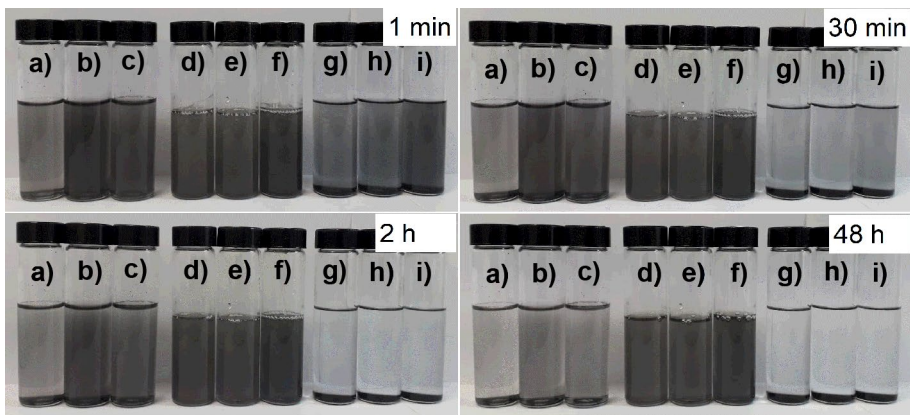

Fig. 6 Dispersion tests using distilled water with **a**) NG, **b**) N-EG, **c**) N-EEG; DGEBA with **d**) NG, **e**)
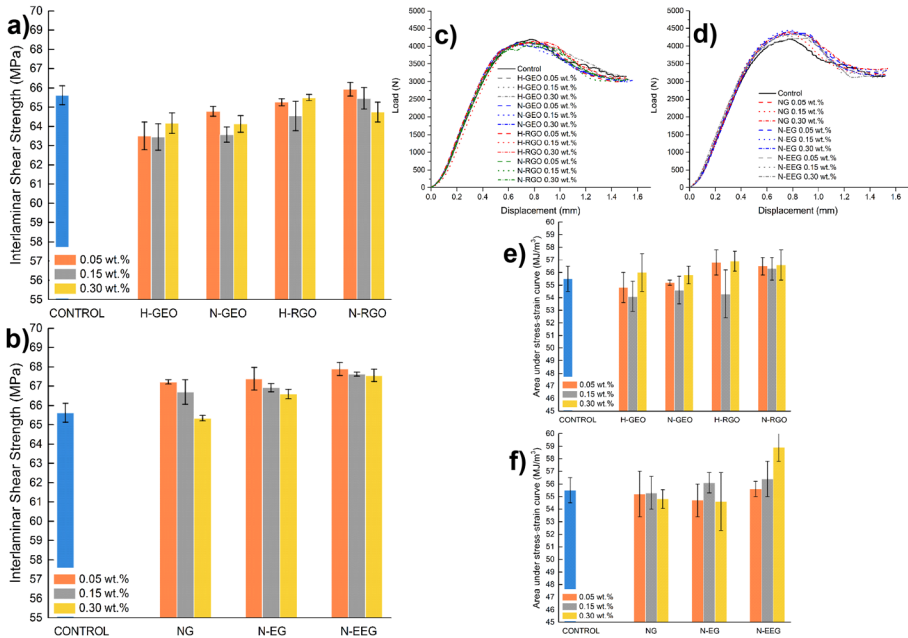N-EG, **f**) N-EEG; and hexane with **g**) NG, **h**) N-EG, **i**) N-EEG

Fig. 7 Interlaminar shear strength of composite laminates reinforced with graphene derivatives obtained by **a**) the chemical methods from two graphite precursors, and **b**) the physical method. Load–displacement curves of composite laminates with graphene derivatives from **c**) chemical methods and **d**) physical method. Area under the stress-strain curves of composites with graphene derivates from e) chemical methods f) physical method

that oxygen groups presented on graphene oxide could bind with the epoxy resin, but in this case, the restricted area of each prepreg limit the contact between every graphene sheet and the resin, and restored layers provide higher effect of reinforcement. Also, some specimens reinforced with graphene derivatives from NG as precursor, have the tendency to overcome those composite laminates reinforced with graphenes obtained from HG on interlaminar shear strength. It is probable that the higher oxygen contained in NG, compared to HG, promoted more exfoliation of the layers increasing the contact area of N-GEO and N-RGO with the surface of each layer of the composite laminates, even when their structure have lower quality. The best performance is observed with N-RGO at the lowest load, inducing the highest interfacial adhesion between layers of the composite. Even though some composite laminates showed lower or equal performance compared to the control specimen (without nanomaterials), it was observed that graphene derivatives produced from natural, inexpensive, even with a less structural quality precursor, exhibit a better performance as reinforcement materials.

The results obtained from short beam tests including graphene derivatives produced by the physical method as reinforcement materials are showed in Fig. 7b. Interesting tendency is found. First, almost all reinforced composite laminates exhibit higher values of interlaminar shear strength compared to the control specimen. Even with NG, some composites showed better performance at low loads, 0.05 and 0.15 wt.%. Specimens at 0.3wt.% of carbon materials show lower ILSS values due to the agglomeration formed on the limited surface of each prepreg during the spraying stage. However, with N-EEG the higher interfacial adhesion in the composite laminates is achieved. Results of this work corroborate

that GNPs may be that expected nanomaterial with high properties and low cost which may be obtained by a feasible scale-up. It is possible to obtain specimens with higher adhesion between layers when graphene derivatives of high thickness and structural quality are included on the interfaces. Besides, according to the results observed in Fig. 7b, quantities as low as 0.05 wt.% of N-EEG are required to reach significative increments on ILSS values. Moreover, energy absorbed before complete failure of composite laminates with these graphene derivatives was increased, according to the observed area under the load–displacement curves [62] (Fig. 7d). Actually, the load–displacement curves show clearly that the energy absorbed by composite laminates with H-GEO, N-GEO, H-RGO, or N-RGO is lower compared even with the control specimen. Furthermore, toughness values for all composite laminates are showed in Fig. 7e-f considering the area under the curves from stress and strain values from flexure as a beam simply supported at two points and loaded at the mid-point. Even when graphene derivatives from chemical methods are formed by a few layers, the highest value of toughness is contributed by N-EEG at 0.30 wt.%, increasing the toughness ~6.1% respect to the control specimen. Therefore, in this case, thickness of nanoreinforcements played an important role, more than their chemical surface. NG, N-EG, and N-EEG, are formed by several layers compared to graphene oxide and reduced graphene oxide, but apparently these hydrophobic materials without significative damage on their graphitic lattice are more suitable for improving interlaminar properties in composite laminates. In fact, in a recent work it was reported that GNPs exhibited superior performance as reinforcement compared to monolayer sheets for thermal conductivity measurements [32]. An overall tendency of graphene derivatives obtained by the physical method is found to improve the interlaminar shear strength of composites as their thickness decreased, N-EEG > N-EG > NG; and they provided a better reinforcement effect than graphene oxide and reduced graphene oxide in the composite laminates. Toughness increased with the decreasing of thickness of graphene derivatives from the physical route and the tendency is clearly observed in Fig. 7e-f. The graphene oxide and reduced graphene oxide also provided increments on toughness, but only ~2.5%, whileas with N-EEG (0.30 wt.% of load) ~6.1% more was calculated, respect to the control specimen. N-EEG obtained from an economical precursor and by easy and environmentally friendly route are a feasible option to improve the interlaminar properties on this kind of composite laminates.

2.7 Delaminated regions micrographs

Lateral fracture zones of different specimens are observed in Fig. 8. After short beam tests, the lateral side of the composite laminates was analyzed to detect the delamination produced by the load applied. Delamination is presented in several sections as it is shown in Fig. 8a. When these slits or cracks are observed in detail for the control specimen, it is exhibited a well defined split with predominantly smooth lateral surfaces (Fig. 8b). Matrix containing fibers is an epoxy resin, which is stiff and presents a brittle failure. However, when graphene derivatives are added the morphology of the cracks changes, as Fig. 8c-f illustrate. A delaminated region of a specimen reinforced with N-GEO at 0.05 wt.% is displayed in Fig. 8c and it is perceived the presence of polymer ridges between the separated surfaces. The presence of graphene derivatives between layers of the composite laminates, foment the energy absorption, and the stress around originates polymer crests which are found in transverse sections to the delaminated surfaces. The incorporation of reduced graphene oxide also promotes the formation of
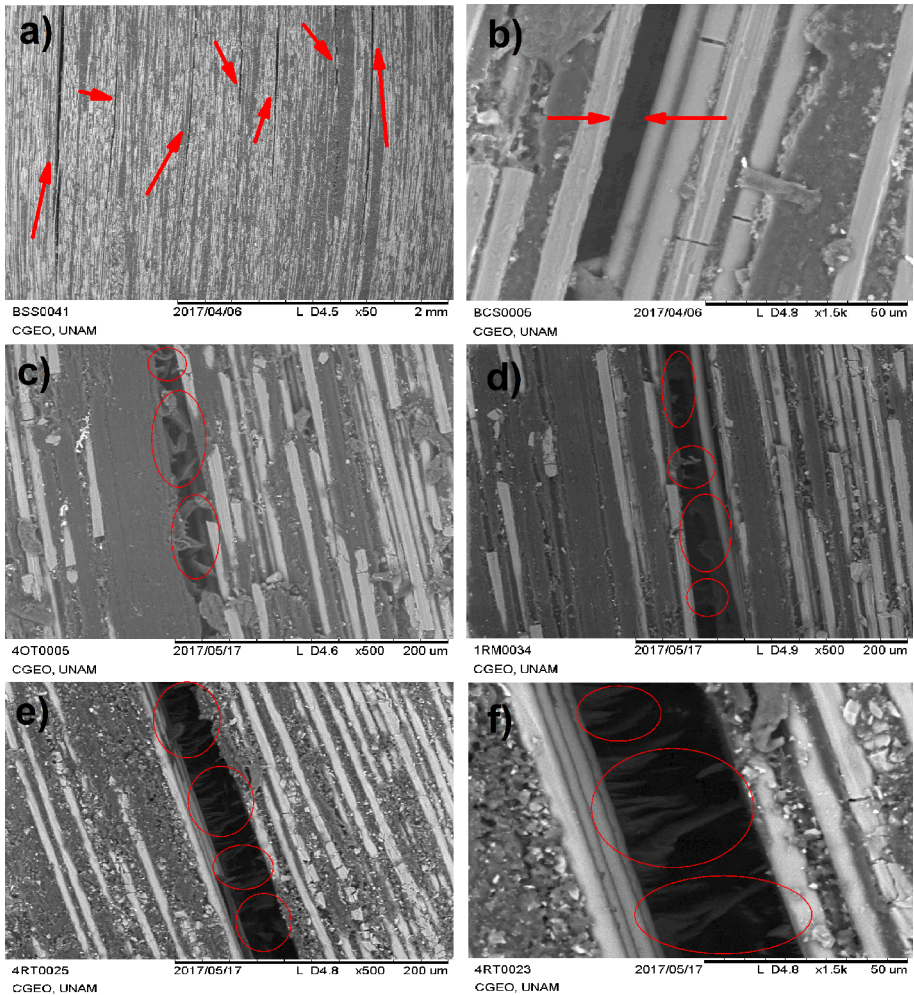
Fig. 8 Delaminated regions of control (**a**, **b**), and specimens reinforcing with **c**) N-GEO at 0.05 wt.%, **d**) H-RGO at 0.05 wt.%, and (**e**, **f**) N-RGO at 0.05 wt.%

polymer crests at the fracture regions, as it is showed in Fig. 8d-f (H-RGO and N-RGO at 0.05 wt.%), regardless of the graphite precursor employed.

On the other hand, Fig. 9a-d displays regions with interlaminar failure of composite laminates reinforced with graphene derivatives obtained by the physical route. The presence of NG, N-EG, and N-EEG at the lowest load, 0.05 wt.% (Fig. 9a-d, respectively), also generate certain degree of plastic deformation. In Fig. 7c-d it was observed that laminate composites exhibit a plastic behavior, and energy absorbed before failure is slightly increased when graphene derivatives from physical method are added, according to the observed area under the load–displacement curves. Also observed is the existence of stretched zones along the fracture regions for all reinforced composite laminates exhibited. Therefore, these kind of materials, shaped by several layers, stimulate

the increment of absorption energy as ILSS results showed, and polymer crests are more evident when N-EEG (0.05 wt.%) is incorporated (Fig. 9c,d).

2.8 Dynamic Mechanical Analysis

Storage moduli (E') variation of specimens reinforced with graphene derivatives obtained by the chemical method is presented in Fig. 10a, b. Storage modulus is associated with the stiffness of the materials [63], in this case, composite laminates. The incorporation of nano-materials on the surface of each prepreg, modified the mobility of matrix polymer chains changing the elastic behavior. The control specimen exhibits an initial E' value of 392 GPa, and with nanomaterials incorporated, important shifts are observed. It is noted that almost the whole specimens reinforced with graphene oxide or reduced graphene oxide enhance their storage modulus, independently of the graphite precursor employed for the obtaining of graphene derivatives. Moreover, the thermal stability of all reinforced composite lami-nates is increased, which can be observed in higher resultant glassy region. These nano-materials increase the stiffness and thermal stability of the composite laminates due to the interfacial interactions and interlocking between the graphene derivatives and the matrix, restricting the mobility of the epoxy chains around their bidimensional and rough surface. In regard to the influence of the graphite precursor, some differences are perceived. At first, the highest E' value at 40 °C is reached adding H-RGO at 0.15 wt.%, ~633 GPa (Fig. 10a), which represents ~61% of increment respect to the control specimen. Nevertheless, the rein-forcement with N-RGO at only 0.05 wt.% produces an enhancement of ~43%, the second
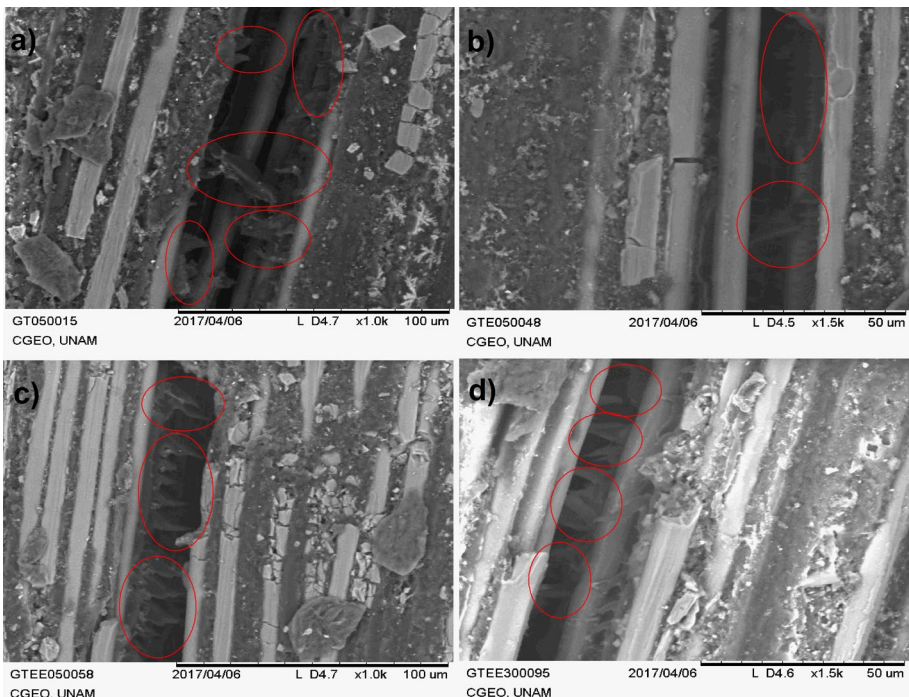

Fig. 9 Interlaminar failure of specimens reinforced with **a**) NG, **b**) N-EG, and (**c, d**) N-EEG at 0.05 wt.%
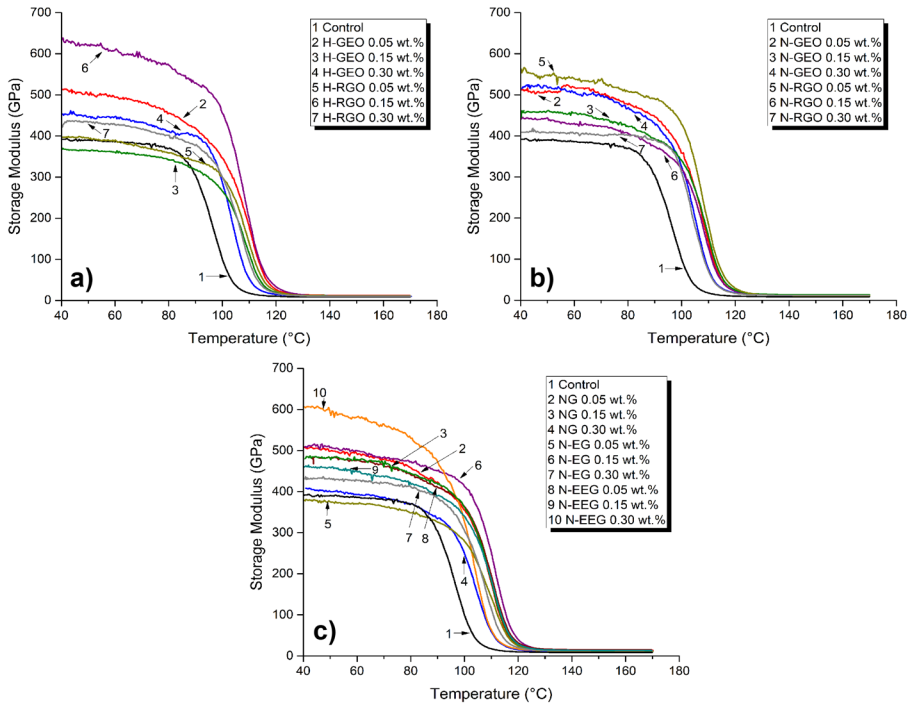
Fig. 10 Storage moduli of composite laminates reinforced with graphene-derivatives produced by the chemical method from **a**) HG and **b**) NG, and **c**) the physical method

highest storage modulus value considering those observed with graphene derivatives prepared by the chemical method (Fig. 10b). Graphene oxide at 0.05 wt.% and 0.30 wt.% from both kind of precursors, also provides notable increments in E'. Although a graphene derivative obtained from HG exhibits the highest storage modulus as reinforcements, it is also observed that some specimens show a similar or even a lower stiffness in contrast to the control, at the beginning of the test (40 °C). As regards the nanosheets prepared from NG, the whole composite laminates with these reinforcements display superior storage moduli compared with the control. However, it results interesting that both reduced graphene oxide, H-RGO and N-RGO (at 0.15 wt.% and 0.05wt.%, respectively), prepared from different kind of graphite, provided the best E' values compared to those reached with graphene oxide. Oxygen is not completely removed from the nanosheets after chemical reduction process, but the diminishing of these groups producing the change of the hydrophilic to hydrophobic character, besides the low loads, caused an excelent effect of reinforcement in the composite laminates. The difference in performance of specimens reinforced with H-RGO (0.15 wt.%) and N-RGO (0.05 wt.%) could be caused by the structure quality of these nanolayers, which also contain distinct quantity of oxygen, as it was observed through IR and Raman spectra. Another important aspect is the incorporation of the graphene derivatives only at the surface of each prepreg by spraying. The nanosheets are not completely immersed in the matrix, their contact with the epoxy polymer chains is limited, nevertheless, the reinforcement effect is outstanding. This latter, also shows the relevance of the effect of nanometric scale in nanosheets over their graphitic quality, indicating N-RGO could be used

efficiently instead of H-RGO, proving that nanometric thickness is more important in this case than high oriented carbon layers. Thus, by this methodology the incorporation of nano-materials improved the initial storage modulus and the glassy region without affecting the stoichiometric ratio between epoxy resin and curing agent, even though some specimens are highly oxygenated. Some studies have shown the presence of graphene oxide in the epoxy resin may alter the cross-linking degree of an epoxy matrix resulting in lower storage moduli [23]. Therefore, it is important the mechanism of reinforcement in this kind of matrix taking account its facility for a posterior production in large scale.

On the other hand, the storage modulus values of composite laminates reinforced with graphene derivatives produced by the physical method are presented in Fig. 10c. Most of the specimens exhibited important increments on E' values and wider glassy region respect to the control specimen. The highest initial storage modulus is obtained adding N-EEG at 0.30 wt.%, reaching until ~ 606 GPa, which is around 55% more than the control. Besides, the reinforcements with N-EG at 0.15 wt.% and NG at 0.05 wt.% are distinguished with storage moduli of ~ 510 and ~ 507 GPa, respectively, indicating that the number of layers of these graphitic nanomaterials has an important influence on the stiffness of the composite laminates. The addition of the thinnest graphene nanoplatelets prepared by this methodology provided a great effect of reinforcement. N-EEG at 0.3 wt.% showed a slight lower performance on interlaminar shear strength tests compared to the others loads (N-EEG at 0.05 and 0.15 wt.%); however, the storage modulus was noticeably increased at this concentration. This could be attributed to the base of each test. In DMA tests an oscillatory stress is applied at a controlled frequency, in a range of temperature; therefore, epoxy chains are slowly rearranged as a response to the test conditions, and the higher load of N-EEG provided a major restriction on the mobility of polymer chains. The higher quantity of nanomaterial of ~ 19 nm of thickness interacts with the polymer chains, which hinders the movement of the epoxy chains and produces a better transference of the stress to N-EEG. This interaction produces a noticeable increment on the storage modulus. Regarding performance of N-EEG at 0.3 wt.% on short beam test, the conditions of the test promote the presence of an excessive interlaminar shear stress while the load increases until fracture takes place. The interlaminar shear stress is deflected by the nanomaterials; however, the higher quantity of N-EGG the more agglomerates are formed, and agglomerates propitiate the interlaminar crack formation. Nevertheless, the increase of ~ 55% in storage modulus, adding N-EEG (0.30 wt.%) is the second highest considering the total composite laminates prepared in this work, including those reinforced with graphene derivatives prepared through the chemical method. It is important to highlight that the structural quality of N-EG and N-EEG is not significatively modifed by the steam explosion and ultrasonic exfoliation, even, the quantity of oxygen remain very similar to that observed in the graphite precursor. Therefore, there are not functional groups to form chemical links between the graphene derivatives from the physical method and the epoxy matrix. However, as it was mentioned previously, the graphenic structure of these nanoplatelets and compatibility with the polymer matrix provide strong interfacial interaction to increase the performance of the composite laminates. This can be supported by the dispersion tests showed in previous sections, where the mixtures prepared with graphene derivatives obtained by the physical route were the darkest implying a better dispersion and good compatibility with epoxy resin. Furthermore, it is important to consider the significant lower cost of NG (compared with HG) and the mentioned advantages of the physical process, which make N-EEG a viable option to satisfy the industrial requirements. Moreover, it is necessary to remark that the thickness of the graphene derivatives evaluated in this work had a marked influence on the interlaminar shear strength and storage moduli. Regarding ILSS results, the

tendency was more evident, because the graphene derivatives of higher thickness exhibited a better performance compared to the control specimen and laminates reinforced with graphene oxide and reduced graphene oxide. As to stiffness, all graphene derivatives, of low and high thickness, contributed to increase the storage modulus; at this conditions, these materials obstructed the mobility of the epoxy chains by an efective interlocking between them. For this test, beside thickness, the additional features of the graphene derivatives influence on storage modulus behavior, due to the interfacial interactions between matrix and reinforcement are affected by the chemical surface of the nanomaterials, dispersion, roughness, and others. However, great results are observed with graphene derivatives of higher thickness.

On the other hand, tan delta curves of composite laminates reinforced with graphene derivatives obtained by chemical and physical methods are showed in Fig. 11a-c. These curves let to detect the glass transition temperature (Tg), which is observed on the peak of tan delta graphics. Moreover, the high of tan delta curves provides important information about the interfacial adhesion between reinforcements and the epoxy matrix around them; weak interfaces are reflected in more energy dissipation [64]. Figure 11a-c exhibts that the high of tan delta peaks of the whole composite laminates remains similar or even lower to that observed in control specimen. This behavior may be attributed to the great interfacial interactions between graphene derivatives employed and the polymer matrix, which obstruct the molecular epoxy movement. The presence of these carbon nanomaterials on the surface of each prepreg result in a reduction of polymer chains motions at their interfaces and therefore, the high of tan delta peaks diminishes. With regard to glass transition
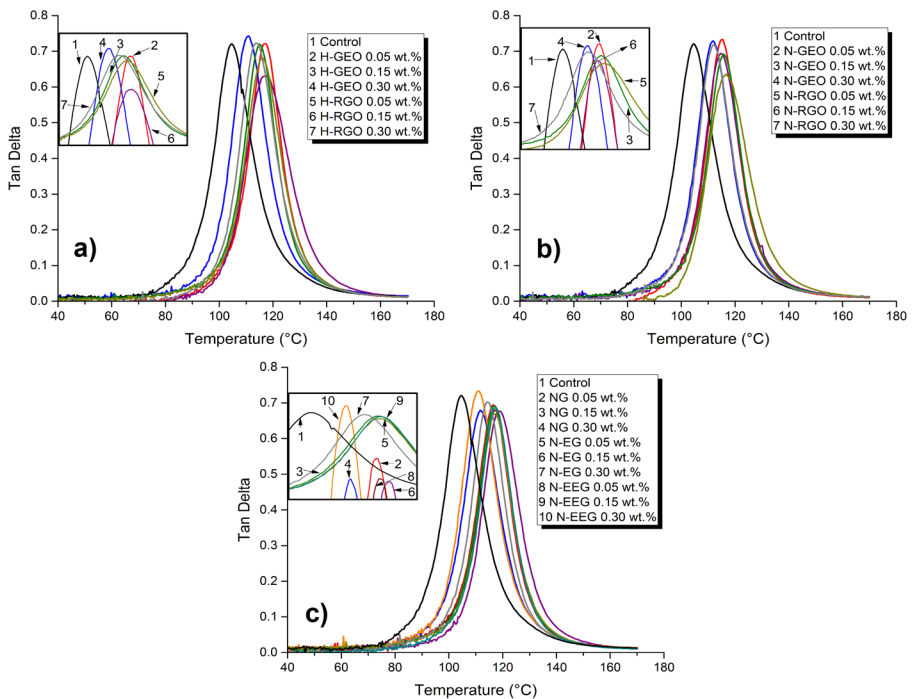

Fig. 11 Tan delta graphs of specimens reinforced with graphene derivatives obtained from **a**) HG, and **b**) NG (chemical method); and, **c**) the physical route
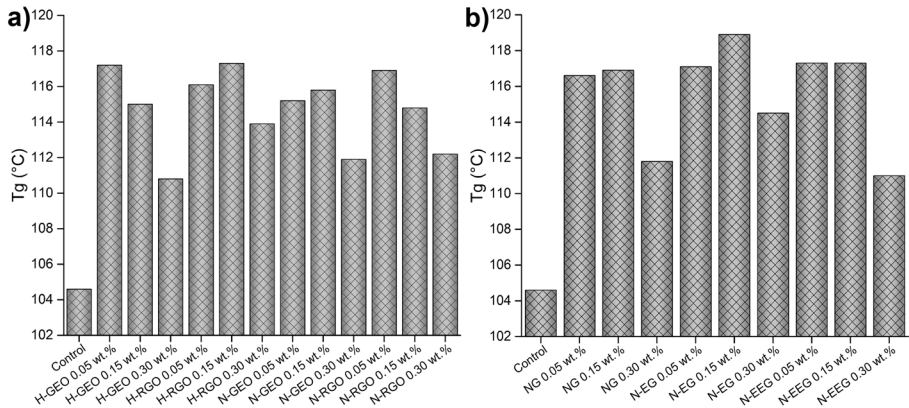
Fig. 12 Tg values of composite laminates reinforced with graphene derivatives obtained by **a**) the chemical method and **b**) the physical method

temperature, Fig. 12a,b exhibits the values of the all composite laminates prepared in this work. Control specimen exhibits a Tg value of ~105 °C, meanwhile all reinforced specimens show remarkable increments. Even though, Tg values from composite laminates reinforced with nanosheets prepared by the chemical method are substantially higher than control sample, more composites reached outstanding Tg adding graphene derivatives obtained by the physical method. Through the incorporation of N-EG at 0.15 wt.%, Tg increases until ~119 °C, which is the highest value obtained in this work. Then, a Tg value of ~117 °C is obtained with the addition of NG (0.05 wt.%), NG (0.15 wt.%), N-EG (0.05 wt.%), N-EEG (0.05 wt.%), and N-EEG (0.15 wt.%). Also, a Tg of 117 °C is obtained reinforcing with H-GEO (0.05 wt.%), H-RGO (0.15 wt.%), and N-RGO (0.05 wt.%). Hence, a great performance can be achieved with graphene derivatives from the physical method. The incorporation of these graphene derivatives on the surface of each prepreg could strengthen and toughen the epoxy matrix immobilizing the polymer chains around the surface of the carbon nanolayers, which produced an remarkable increment in Tg.

3 Conclusions

Graphene derivatives produced by chemical and physical methods, were evaluated as reinforcements materials in composite laminates. Furthermore, two graphite precursors were employed to prepare graphene derivatives through the chemical method. Some different oxygen groups were generated on graphene oxide from highly oriented graphite in comparison to natural graphite. For reduced graphene oxide, through IR spectra it was observed that oxygen remained, which by the bands observed, is higher for derivatives from natural graphite. The lower oriented structure and initial oxygen content on NG could foment the additional oxygen quantity attached on its graphitic lattice. Regarding the chemical and physical methods, remarkable features were found. The chemical method causes damages to the graphitic structure and oxygen groups are generated as a result of oxydation process; even, after chemical reduction, restoration of the graphitic domain is partial. On the other hand, the physical method through steam explosion and ultrasonication, produced materials

with structural quality similar to the graphite precursor. No additional oxygen groups were generated by the process and exfoliation was successful in obtaining graphene nanoplatelets around 19 nm of thickness. Moreover, dispersion tests showed that N-EG and N-EEG were efectively dispersed in epoxy resin obtaining the darkest mixtures, which reimained stable during all the time.

As reinforcing materials in the composite laminates, there are no prominent differences between graphenic nanomaterials obtained by the chemical method from HG and NG, indicating that nanometric thickness effect of nanosheets prevails over their orientation and graphitization at interface level. On the other hand, it was found that graphene derivatives produced by the physical method overcome those by chemical routes in interlaminar shear strength. It is probable that the less structural damage resulting of explosion and exfoliation steps played an important factor on their performance. In addittion, these reinforcements were favorable for increasing the interlaminar shear strength, implying a better compatibility between components and the matrix. Regard to thermo mechanical properties, the highest storage modulus was increased ~ 61% adding H-RGO at 0.15 wt.%; however, the incorporation of N-EEG at 0.30 wt.% produced an increment of ~ 55%, the second highest storage modulus considering the whole composite laminates. Moreover, the reinforcement with graphene derivatives obtained by the physical method, produced the highest improvement in Tg values. In fact, most of the composite laminates with NG, N-EG, and N-EEG showed the highest Tg values, around 117–119 °C. This work shows that graphene derivatives which are formed by higher thickness, are able to increase the performance of composite laminates, even in higher degree in some tests than those prepared by typical chemical methods, like graphene oxide and reduced graphene oxide. It would be relevant to modify the process conditions of this physical method (proposed in this research) to obtain graphene derivatives with a wider range of thickness and find the best value to improve the properties of these composite laminates. At these experimental conditions, N-EG and N-EEG showed better effect as reinforcement than NG; but it was necessary to determine the influence of starting graphite as reference. Nevertheless, a decrease in thickness of graphene derivatives from the physical method modified the interfacial adhesion of the final composites respect to those with H-GEO, N-GEO, H-RGO, N-RGO and control specimen. Graphene derivatives obtained by steam explosion and ultrasonic exfoliation represent a viable option as reinforcement materials, due to the easy and environmental friendly production, low cost of the graphite precursor, possibility of large-scale production, high structure quality and good performance in composite laminates.

4 Data availability statement:

Reserved DOI**:** https://doi.org/10.17632/4zwmrfvgsb.1

Declarations

Conflicts of interest The authors declare no conflicts of interest.

References

1. Mohan, V.B., Laub, K.-T., Huic, D., Bhattacharyy, D.: Graphene-based materials and their composites: A review on production, applications and product limitations. Compos. Part B Eng. **142**, 200–220 (2018)
2. Grayfer, E.D., Makotchenkom, V.G., Nazarov, A.S., Kim, S.-J., Fedorov, V.E.: Graphene: chemical approaches to the synthesis and modification. Russ. Che. Rev. **80**, 751–770 (2011)
3. Kattimuttathu, S.I., Krishnappan, C., Vellorathekkaepadil, V., Nutenki, R., Mandapati, V.R.: Cernik, M Synthesis, characterization and optical properties of graphene oxide-polystyrene nanocomposites. Polym. Adv. Technol. **26**, 214–222 (2015)
4. Mao, S., Pu, H., Chen, J.: Graphene oxide and its reduction: modeling and experimental progress. RSC Adv. **2**, 2643–2662 (2012)
5. Zhu, J., Shentu, X., Xu, X., Zheng, A., Guan, Y., Wei, D.: Preparation of graphene oxide modified glass fibers and their application in flame retardant polyamide 6. Polym. Adv. Technol. **31**, 1709–1718 (2020)
6. Zhu, B.Y., Murali, S., Cai, W., Li, X., Suk, J.W., Potts, J.R., Ruoff, R.S.: Graphene and graphene oxide: synthesis, properties, and applications. Adv. Mater. **22**, 3906–3924 (2010)
7. Haubner, K., Murawski, J., Olk, P., Eng, L.M., Ziegler, C., Adolphi, B., Jaehne, E.: The route to functional graphene oxide. ChemPhysChem **11**, 2131–2139 (2010)
8. Kausar, A., Rafique, I., Anwar, Z., Muhammad, B.: Perspectives of Epoxy/Graphene Oxide Composite: Significant Features and Technical Applications. Polym. Plast. Technol. Eng. **55**, 704–722 (2016)
9. Zhang, L., Jiao, H., Jiu, H., Chang, J., Zhang, S., Zhao, Y.: Thermal, mechanical and electrical properties of polyurethane/(3-aminopropyl) triethoxysilane functionalized graphene/epoxy resin interpenetrating shape memory polymer composites. Compos. Part A: Appl. Sci. Manufact. **90**, 286–295 (2016)
10. Sreenivasulu, B., Ramji, B.R., Nagaral, M.: A Review on Graphene Reinforced Polymer Matrix Composites. Mater. Today: Proc. **5**, 2419–2428 (2018)
11. Phiri, J., Gane, P., Maloney, T.C.: General overview of graphene: Production, properties and application in polymer composites. Mat. Sci. Eng. B Adv. **215**, 9–28 (2017)
12. Thema, F.T., Moloto, M.J., Dikio, E.D., Nyangiwe, N.N., Kotsedi, L., Maaza, M., Khenfouch, M.: Synthesis and characterization of graphene thin films by chemical reduction of exfoliated and intercalated graphite oxide. J. Chem. **2013**, 1–6 (2013)
13. Huang, X., Yin, Z.: Graphene-based materials: synthesis, characterization, properties, and applications. Small **14**, 1876–1902 (2011)
14. Smith, A.T., LaChance, A.M., Zeng, S., Liu, B., Sun, L.: Synthesis, properties, and applications of graphene oxide/reduced graphene oxide and their nanocomposites. Nano Mater. Sci. **1**, 31–47 (2019)
15. Papageorgiou, D.G., Kinloch, I.A., Young, R.J.: Mechanical properties of graphene and graphene-based Nanocomposites. Prog. Mater. Sci. **90**, 75–127 (2017)
16. Del Río, F., Boado, M.G., Rama, A., Guitián, F.: A comparative study on different aqueous-phase graphite exfoliation methods for few-layer graphene production and its application in alumina matrix composites. J. Eur. Ceram. Soc. **37**, 3681–3693 (2017)
17. Amiri, A., Zubir, M.N.M., Dimiev, A.M., Teng, K.H., Shanbedi, M., Kazi, S.N., BinRozali, S.: Facile, environmentally friendly, cost effective and scalable production of few-layered graphene. Chem. Eng. J. **326**, 1105–1115 (2017)
18. Antunes, M., Gedler, G., Abbasi, H., Velasco, J.I.: Graphene nanoplatelets as a multifunctional filler for polymer foams. Mater. Today: Proc. **3**, S233–S239 (2016)
19. Arao, Y., Mori, F., Kubouchi, M.: Efficient solvent systems for improving production of few-layer graphene in liquid phase exfoliation. Carbon **118**, 18–24 (2017)
20. Wei, Y., Sun, Z.: Liquid-phase exfoliation of graphite for mass production of pristine few-layer graphene. Curr. Opin. Colloid Interface Sci. 20311–321 (2015)
21. Yu, Z., Zhang, B., Yu, F., Xu, G., Song, A.: A real explosion: The requirement of steam explosion pretreatment. Bioresour. Technol. **121**, 335–341 (2012)

22. Wang, H., Zhang, S., Yu, K., Yue, C., Liu, M., Bao, C.: Studies on the mechanism for the sudden mechanical property drops of graphene/polymer nanocomposites. Polym. Adv. Technol. **31**, 786–794 (2020)

23. Ramos-Galicia, L., Martínez-Hernandez, A.L., Fuentes-Ramirez, R., Velasco-Santos, C.: 1D and 2D oxidized carbon nanomaterials on epoxy matrix: performance of composites over the same processing conditions. Mater. Res. Express **4**, 115604 (2017)

24. Shah, R., Kausar, A., Muhammad, B., Sayed, S.: Progression from graphene and graphene oxide to high performance polymer-based nanocomposite: a review. Polym. Plast. Technol. Eng. **54**, 173–183 (2015)

25. Poutrel, Q.A., Wang, Z., Wang, D., Soutis, C., Gresil, M.: Effect of pre and Post-Dispersion on Electro-Thermo-Mechanical Properties of a Graphene Enhanced Epoxy. Appl. Compos. Mater. **24**, 313–336 (2017)

26. Pullicino, E., Zou, W., Gresil, M., Soutis, C.: The Effect of Shear Mixing Speed and Time on the Mechanical Properties of GNP/Epoxy Composites. Appl. Compos. Mater. **24**, 301–311 (2017)

27. Prusty, R.K., Ghosh, S.K., Rathore, D.K., Ray, B.C.: Reinforcement effect of graphene oxide in glass fibre/epoxy composites at in-situ elevated temperature environments: An emphasis on graphene oxide content. Compos. Part A: Appl. Sci. Manufact. **95**, 40–53 (2017)

28. Mannov, E., Schmutzler, H., Chandrasekaran, S., Viets, C., Buschhorn, S., Tölle, F., Mülhaupt, R., Schulte, K.: Improvement of compressive strength after impact in fibre reinforced polymer composites by matrix modification with thermally reduced graphene oxide. Compos. Sci. Technol. **87**, 36–41 (2013)

29. Rodríguez-González, J.A., Rubio-González, C., Ku-Herrera, J.J., Ramos-Galicia, L., Velasco-Santos, C.: Effect of seawater ageing on interlaminar fracture toughness of carbon fiber/epoxy composites containing carbon nanofillers. J. Reinf. Plast. Compos. **37**, 1346–1359 (2018)

30. Zeng, L., Liu, X., Chen, X., Soutis, C.: Surface Modification of Aramid Fibres with Graphene Oxide for Interface Improvement in Composites. Appl. Compos. Mater. **25**, 843–852 (2018)

31. Jia, J., Du, X., Chen, C., Sun, X., Mai, Y.-W., Kim, J.K.: 3D network graphene interlayer for excellent interlaminar toughness and strength in fiber reinforced composites. Carbon **95**, 978–986 (2015)

32. Wang, F., Cai, X.: Improvement of mechanical properties and thermal conductivity of carbon fiber laminated composites through depositing graphene nanoplatelets on fibers. J. Mater. Sci. **54**, 3847–3862 (2019)

33. Liu, K., Macosko, C.W.: Can nanoparticle toughen fiber-reinforced thermosetting polymers? J. Mater. Sci. **54**, 4471–4483 (2019)

34. Umer, R., Li, Y., Dong, Y., Haroosh, H.J., Liao, K.: The effect of graphene oxide (GO) nanoparticles on the processing of epoxy/glass fiber composites using resin infusion. Int. J. Adv. Manuf. Technol. **81**, 2183–2192 (2015)

35. Kamar, N.T., Hossain, M.M., Khomenko, A., Haq, M., Drzal, L.T., Loos, A.: Interlaminar reinforcement of glass fiber/epoxy composites with graphene nanoplatelets. Compos. Part A: Appl. Sci. Manufact. **70**, 82–92 (2015)

36. Chen, J., Zhao, D., Jin, X., Wang, C., Wang, D., Ge, H.: Modifying glass fibers with graphene oxide: Towards high-performance polymer composites. Compos. Sci. Technol. **97**, 41–45 (2014)

37. Rodríguez-González, J.A., Rubio-González, C., Jiménez-Mora, M., Ramos-Galicia, L., Velasco-Santos, C.: Influence of the Hybrid Combination of Multiwalled Carbon Nanotubes and Graphene Oxide on Interlaminar Mechanical Properties of Carbon Fiber/Epoxy Laminates. Appl. Compos. Mater. **25**, 1115–1131 (2018)

38. Wang, F., Drzal, L.T., Qin, Y., Huang, Z.: Size effect of graphene nanoplatelets on the morphology and mechanical behavior of glass fiber/epoxy composites. J. Mater. Sci. **51**, 3337–3348 (2016)

39. Domun, N., Paton, K.R., Blackman, B.R.K., Kaboglu, C., Vahid, S., Zhang, T., Dear, J.P., Kinloch, A.J., Hadavinia, H.: On the extent of fracture toughness transfer from 1D/2D nanomodified epoxy matrices to glass fibre composites. J. Mater. Sci. **55**, 4717–4733 (2020)

40. Anwar, Z., Kausar, A., Rafique, I., Muhammad, B.: Advances in Epoxy/Graphene Nanoplatelet Composite with Enhanced Physical Properties: A Review. Polym. Plast. Technol. Eng. **55**, 643–662 (2015)

41. Kausar, A., Anwar, Z., Muhammad, B.: Recent Developments in Epoxy/Graphite, Epoxy/Graphene and Epoxy/Graphene Nanoplatelet Composites: A Comparative Review. Polym. Plast. Technol. Eng. **55**, 1192–1210 (2016)

42. Ning, H., Li, J., Hu, N., Yan, C., Liu, Y., Wu, L., Liu, F., Zhang, J.: Interlaminar mechanical properties of carbon fiber reinforced plastic laminates modified with graphene oxide interleaf. Carbon **91**, 224–233 (2015)

43. Liu, L., Xiao, L., Zhang, X., Li, M., Chang, Y., Shang, L., Ao, Y.: Improvement of the thermal conductivity and friction performance of poly(ether ether ketone)/carbon fiber laminates by addition of graphene. RSC Adv. **5**, 57853–57859 (2015)

44. Hsieh, T.-H., Chen, W.-J., Chiang, C.-L., Shen, M.-Y.: Environmental aging effect on interlaminar properties of graphene nanoplatelets reinforced epoxy/carbon fiber composite laminates. J. Reinf. Plast. Compos. **37**, 1177–1190 (2018)

45. Subha, S., Krishna, B.S., Singh, D., Gokulnath, R.: Effect of Graphene Platelets/Fiber on Plastics Nanocomposites under Low-Velocity Impact Response. Appl. Mech. Mater. **852**, 23–28 (2016)

46. Du, X., Zhou, H., Sun, W., Liu, H.Y., Zhou, G., Zhou, H., Mai, Y.W.: Graphene/epoxy interleaves for delamination toughening and monitoring of crack damage in carbon fibre/epoxy composite laminates. Compos. Sci. Technol. **140**, 123–133 (2017)

47. Han, X., Zhao, Y., Sun, J.J.M., Li, Y., Zhang, J.J.D., Hao, Y.: Effect of graphene oxide addition on the interlaminar shear property of carbon fiber fiber-reinforced epoxy composites. New Carbon Mater. **32**, 48–55 (2017)

48. Li, Y., Zhang, H., Huang, Z., Bilotti, E., Peijs, T.: Graphite Nanoplatelet Modified Epoxy Resin for Carbon Fibre Reinforced Plastics with Enhanced Properties. J. Nanomater. (Article ID 5194872), 1–10 (2017)

49. Yao, X., Gao, X., Jiang, J., Xu, C., Deng, C., Wang, J.: Comparison of carbon nanotubes and graphene oxide coated carbon fiber for improving the interfacial properties of carbon fiber/epoxy composites. Compos. Part B **132**, 170–177 (2018)

50. Cheng, X., Zhang, J., Wang, H., Wu, L., Sun, Q.: Improving the interlaminar shear strength and thermal conductivity of carbon fiber/epoxy laminates by utilizing the graphene-coated carbon fiber. J. Appl. Polym. Sci. **136**, 47061 (2019)

51. Rafiee, M., Nitzsche, F., Laliberte, J., Hind, S., Robitaille, F., Labrosse, M.R.: Thermal properties of doubly reinforced fiberglass/epoxy composites with graphene nanoplatelets, graphene oxide and reduced-graphene oxide. Compos. Part B **164**, 1–9 (2019)

52. Ashori, A., Ghiyasi, M., Fallah, A.: Glass fiber-reinforced epoxy composite with surface-modified graphene oxide: enhancement of interlaminar fracture toughness and thermo-mechanical performance. Polym. Bull. **76**, 259–270 (2019)

53. Senis, E.C., Golosnoy, I.O., Dulieu-Barton, J.M., Thomsen, O.T.: Enhancement of the electrical and thermal properties of unidirectional carbon fibre/epoxy laminates through the addition of graphene oxide. J. Mater. Sci. **54**, 8955–8970 (2019)

54. De la Luz-Asunción, M., Sánchez-Mendieta, V., Martínez-Hernández, A.L., Castaño, V.M., Velasco-Santos, C.: Adsorption of Phenol from Aqueous Solutions by Carbon Nanomaterials of One and Two Dimensions: Kinetic and Equilibrium Studies. J. Nanomater. (Article ID 405036), 1–14 (2015)

55. Ramos-Galicia, L., Perez-Ramirez, E.E., Fuentes-Ramirez, R., Martinez-Hernandez, A.L., Velasco-Santos, C.: Carbon Nanotubes and Reduced Graphene Oxide's Dimensionality Effect on Thermoset Matrix Performance. Mater. Perform. Charact. **8**, 434–447 (2019)

56. Zaman, I., Phan, T.T., Kuan, H.-C., Meng, Q., La, L.T.B., Luong, L., Youssf, O., Ma, J.: Epoxy/Graphene platelets nanocomposites with two levels of interface strength. Polymer **52**, 1603–1611 (2011)

57. Rozada, R., Paredes, J.I., Villar-Rodil, S., Martínez-Alonso, A., Tascón, J.M.D.: From graphene oxide to pristine graphene: revealing the inner workings of the full structural restoration. Nanoscale **7**, 2374–2390 (2015)

58. Cooper, D.R., D'Anjou, B., Ghattamaneni, N., Harack, B., Hilke, M., Horth, A., Majlis, N., Massicotte, M., Vandsburger, L., Whiteway, E., Yu, V.: Experimental Review of Graphene. ISRN Condens. Matter. Phys. (Article ID 501686) 1–56 (2012)

59. Stankovich, S., Dikin, D.A., Piner, R.D., Kohlhaas, K.A., Kleinhammes, A., Jia, Y., Wu, Y., Nguyen, S.B.T., Ruoff, R.S.: Synthesis of graphene-based nanosheets via chemical reduction of exfoliated graphite oxide. Carbon **45**, 1558–1565 (2007)

60. Gharib, D.H., Gietman, S., Malherbe, F., Moulton, S.E.: High yield, solid exfoliation and liquid dispersion of graphite driven by a donor-acceptor interaction. Carbon **123**, 695–707 (2017)

61. Yavas, D., Zhang, Z., Liu, Q., Wu, D.: Interlaminar shear behavior of continuous and short carbon fiber reinforced polymer composites fabricated by additive manufacturing. Compos. Part B. **204**, 108460 (2021)

62. Shinde, D.K., Kelkar, A.D.: Short beam strength of laminates fiberglass composite with and without electospun TEOS nanofibers. Conference SAMPE 2016, LB15–0062 (2016)

63. Rahman, M.M., Zainuddin, S., Hosur, M.V., Malone, J.E., Salam, M.B.A., Kumar, A., Jeelani, S.: Improvements in mechanical and thermo-mechanical properties of e-glass/epoxy composites using amino functionalized MWCNTs. Compos. Struct. **94**, 2397–2406 (2012)
64. Keusch, S., Haessler, R.: Influence of surface treatment of glass fibres on the dynamic mechanical properties of epoxy resin composites. Compos. Part A: Appl. Sci. Manufact. **30**, 997–1002 (1999)